

## The late-time light curve of the type Ia supernova 2000cx<sup>★,★★</sup>

J. Sollerman<sup>1</sup>, J. Lindahl<sup>1,2</sup>, C. Kozma<sup>1</sup>, P. Challis<sup>3</sup>, A. V. Filippenko<sup>4</sup>, C. Fransson<sup>1</sup>, P. M. Garnavich<sup>5</sup>,  
B. Leibundgut<sup>6</sup>, W. Li<sup>4</sup>, P. Lundqvist<sup>1</sup>, P. Milne<sup>7</sup>, J. Spyromilio<sup>6</sup>, and R. P. Kirshner<sup>3</sup>

<sup>1</sup> Stockholm Observatory, AlbaNova, Department of Astronomy, 106 91 Stockholm, Sweden  
e-mail: jesper@astro.su.se

<sup>2</sup> Onsala Space Observatory, Chalmers University of Technology, 439 92 Onsala, Sweden

<sup>3</sup> Harvard-Smithsonian Center for Astrophysics, 60 Garden Street, Cambridge, MA 02138, USA

<sup>4</sup> Department of Astronomy, University of California, Berkeley, CA 94720-3411, USA

<sup>5</sup> Physics Department, University of Notre Dame, Notre Dame, IN 46566, USA

<sup>6</sup> European Southern Observatory, Karl-Schwarzschild-Strasse 2, 85748 Garching, Germany

<sup>7</sup> Steward Observatory, University of Arizona, 933 North Cherry Avenue, Tucson, AZ 85721, USA

Received 19 May 2004 / Accepted 11 August 2004

**Abstract.** We have conducted a systematic and comprehensive monitoring programme of the type Ia supernova 2000cx at late phases using the VLT and *HST*. The VLT observations cover phases 360 to 480 days past maximum brightness and include photometry in the *BVRJH* bands, together with a single epoch in each of *U* and *K<sub>s</sub>*. While the optical bands decay by about 1.4 mag per 100 days, we find that the near-IR magnitudes stay virtually constant during the observed period. This means that the importance of the near-IR to the bolometric light curve increases with time. The finding is also in agreement with our detailed modeling of a type Ia supernova in the nebular phase. In these models, the increased importance of the near-IR is a temperature effect. We note that this complicates late-time studies where often only the *V* band is well monitored. In particular, it is not correct to assume that any optical band follows the bolometric light curve at these phases, and any conclusions based on such assumptions, e.g., regarding positron-escape, must be regarded as premature. A very simple model where all positrons are trapped can reasonably well account for the observations. The nickel mass deduced from the positron tail of this light curve is lower than found from the peak brightness, providing an estimate of the fraction of late-time emission that is outside of the observed wavelength range. Our detailed models show the signature of an infrared catastrophe at these epochs, which is not supported by the observations.

**Key words.** stars: supernovae: general – stars: supernovae: individual: SN 2000cx

### 1. Introduction

Type Ia supernovae (SNe Ia) are believed to be the destructive thermonuclear explosions of white dwarfs (e.g., Hoyle & Fowler 1960; see for a review Leibundgut 2000). During the first years, their light curves are powered by the radioactive decay of freshly nucleosynthesized <sup>56</sup>Ni, releasing MeV  $\gamma$ -rays and positrons in the ejecta. The uniformity of the early-time light curves has enabled the use of SNe Ia for measuring cosmological distances (Schmidt et al. 1998; Riess et al. 1998; Perlmutter et al. 1999).

The peak luminosity of such an explosion is given by the amount of ejected <sup>56</sup>Ni, and the early bolometric light curve

can thus be used to determine this important quantity (Arnett 1982; Contardo et al. 2000). The shape of the light curve at the early post-maximum phase (40–120 days past explosion) is determined by the fraction of the  $\gamma$ -rays that are thermalized. While the massive type II SNe (like SN 1987A) generally trap most  $\gamma$ -rays, resulting in late-time light curves tracking the radioactive decay of 0.98 mag per 100 days, the light curves of SNe Ia decline much faster. This is because the small progenitor masses and the high expansion velocities of SNe Ia quickly make the ejecta transparent to the  $\gamma$ -rays.

At phases later than about 200 days past the explosion, virtually all  $\gamma$ -rays escape freely from the ejecta, and the luminosity is then provided by the kinetic energy deposited by the positrons. Whether or not the positrons are able to escape from the ejecta depends on the strength and geometry of the magnetic field (Colgate et al. 1980; Ruiz-Lapuente & Spruit 1998; Milne et al. 1999, 2001). While a weak and radially combed magnetic field might allow an increasing fraction of the positrons to escape, thus providing a steep light curve, a

\* Based on observations collected at the European Southern Observatory, Paranal, Chile (ESO Programmes 67.D-0134 and 68.D-0114). Also based in part on observations with the NASA/ESA *Hubble Space Telescope*. These *HST* observations are associated with proposals GO-8602 and GO-9114.

\*\* Tables 1, 2, 4 and 5 are only available in electronic form at <http://www.edpsciences.org>

strong, tangled magnetic field would efficiently trap all the positrons, and keep the light curve at the radioactive decay rate.

The study of the positron phase of the light curve could thus potentially help answer questions about the magnetic field configuration in exploding white dwarfs, as well as to constrain the contribution of supernova explosions to the diffuse Galactic 511 keV background. Previous attempts to study the positron phase of the light curve have, however, been hampered by the lack of both observational data and detailed modeling.

As a first step to investigate whether observations of the positron phase can establish any conclusions about positron escape, we have attempted a photometric study at late phases of the type Ia SN 2000cx, and modeled its light curve in some detail.

### 1.1. SN 2000cx

SN 2000cx was discovered on 17.5 July 2000 (Yu et al. 2000; UT dates are used throughout our paper). It was located  $23^{\circ}0'$  west and  $109^{\circ}3'$  south of the nucleus of the S0 galaxy NGC 524. It was classified as a SN Ia, with a spectrum resembling that of the peculiar SN 1991T (Chornock et al. 2000; see Filippenko 1997, for a review of supernova spectra). The recession velocity of NGC 524 is only  $\sim 2400$  km s $^{-1}$ , and SN 2000cx became the brightest supernova observed that year. Furthermore, the favorable position far from the galaxy center made it a good target for late-time photometry. The early-time photometry has been extremely well covered by Li et al. (2001) and by Candia et al. (2003). The *B*-band maximum occurred on July 26.3 (MJD 51 752.2) at  $B = 13.42$  mag. The early decline rate was determined to be  $\Delta m_{15}(B) = 0.93$  (Li et al. 2001). The light curve around peak was rather unusual. It was a fast riser but a slow decliner (Li et al. 2001), and SN 2000cx has therefore been labeled a peculiar supernova. The unusual early light curve may have been related to the presence of high-velocity material (Branch et al. 2004).

Here we report on our late-time observations of SN 2000cx obtained with the Very Large Telescope (VLT) and the *Hubble Space Telescope* (*HST*). Preliminary results have been reported by Sollerman et al. (2004) and the results presented here supersede that report. The observations, data reduction, and photometry are described in Sect. 2. The results are presented in Sect. 3, and in Sect. 4 we discuss the late-time light curves of SNe Ia in general. In Sect. 5 we describe our detailed modeling, and Sect. 6 discusses the modeling in conjunction with the data. Our main conclusions are summarized in Sect. 7.

## 2. Observations and data analysis

### 2.1. Optical imaging with the VLT

The field of SN 2000cx was observed in the optical (*UBVRI*) range during several epochs between 359 and 480 days past maximum light. These observations were obtained with the Focal Reducer and low dispersion Spectrograph (FORS) instruments<sup>1</sup> at the European Southern Observatory (ESO) VLT.

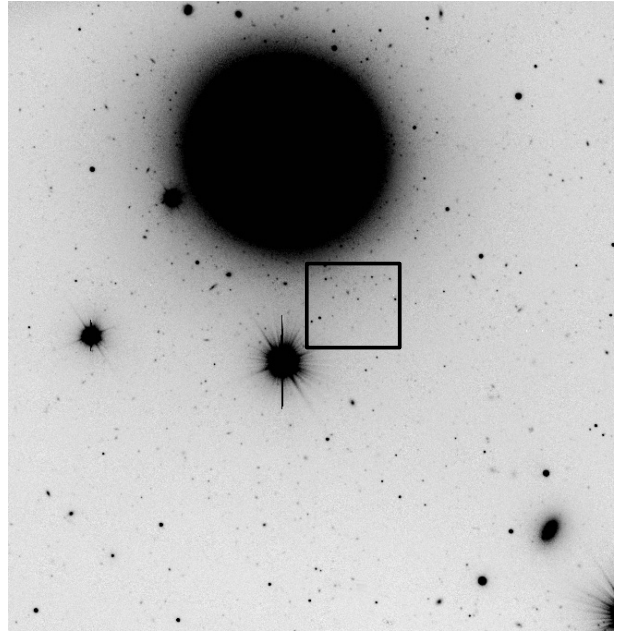


**Fig. 1.** V-band image obtained with VLT/FORS on 21 July 2001, 359 days past maximum light. This is basically the full FORS field of view,  $6.8' \times 6.8'$ . North is up and east to the left. The supernova is  $23''$  west and  $109''$  south of the nucleus of NGC 524. The region containing the supernova is marked by a rectangle, and shown in detail in Fig. 2.

FORS2 was used for the first epoch of observations. This instrument was attached to the fourth of the four VLT Unit telescopes (UT4). The subsequent observations were all conducted with FORS1, which was then mounted at the Cassegrain focus of UT3. A log of the observations is given in Table 1.

Both of the FORS instruments were equipped with  $2048 \times 2048$  pixel CCDs having  $24 \mu\text{m}$  pixels. We used the standard resolution mode that gives a field-of-view of  $6'.8 \times 6'.8$  with a pixel size on the sky of  $0'.20$ . An image of the field of the supernova is displayed in Fig. 1, and a detail of the region around the supernova is shown in Fig. 2.

All observations were split into several exposures with small telescope shifts in between. This was to avoid heavy saturation of a nearby bright star, and to allow for removal of cosmic rays. The observations were all conducted in service mode by the Paranal staff.

The data were reduced with the NOAO IRAF software<sup>2</sup>. We have bias-subtracted and twilight-sky flattened all the frames and then combined the exposures in the same filters using a sigma clipping rejection.

Our first and last epochs of observation were photometric and on the first epoch we observed the following standard fields of Landolt (1992) with FORS2: Mark A, PG 1323-086, PG 2331+055, and SA 109-949. There were in total 15 stars useful for obtaining the photometric solutions in these fields. The instrumental magnitudes of the standard stars were all measured with an aperture of 15 pixel radius. The sky background was estimated using an annulus of inner radius

<sup>1</sup> <http://www.eso.org/instruments/fors1/>

<sup>2</sup> IRAF, <http://iraf.noao.edu/iraf/web/>, is distributed by NOAO.

**Table 3.** Late-time optical magnitudes of SN 2000cx.

MJD <sup>a</sup> 52 000+	Phase <sup>b</sup> (days)	<i>U</i>	<i>B</i>	<i>V</i>	<i>R</i>	<i>I</i>
111.4	359	22.30 (0.08)	21.27 (0.03)	21.28 (0.01)	22.17 (0.02)	21.70 (0.03)
112.3	360			21.28 (0.03)		
165.3	413		22.00 (0.03)	22.02 (0.03)	22.91 (0.03)	22.09 (0.03)
192.1	440				23.26 (0.04)	
199.2	447		22.50 (0.03)	22.46 (0.01)		22.42 (0.03)
201.2	449				23.46 (0.03)	
232.5	480		23.00 (0.04)	23.03 (0.02)	23.85 (0.06)	22.84 (0.05)

<sup>a</sup> Refers to the first exposure.

<sup>b</sup> Days past maximum *B*-band light.

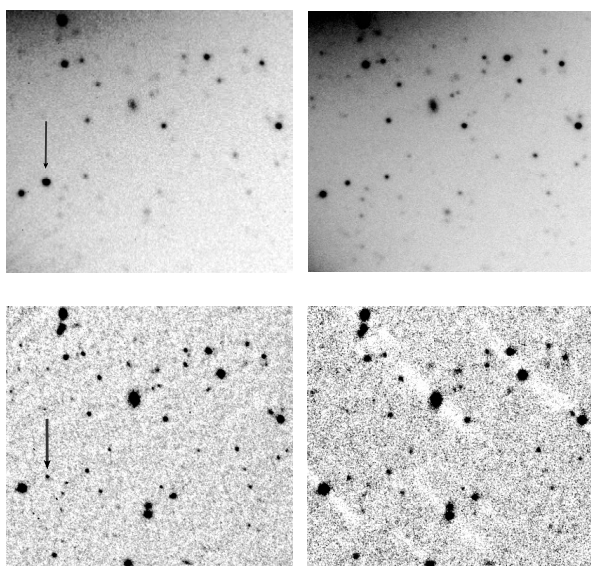


**Fig. 2.** *Upper left:* close-up of the region indicated in Fig. 1, *V* band at 359 days past maximum. The field of view is  $60'' \times 55''$ . North is up and east to the left. SN 2000cx is marked with an arrow. *Upper right:* *V*-band image obtained 480 days past maximum. Note how the supernova has faded considerably compared to the nearby stars. *Lower left:* *J*-band image obtained with VLT/ISAAC 369 days past maximum light. The orientation and field of view is the same as for the optical image above. The supernova is marked with an arrow. *Lower right:* *J*-band image obtained 480 days past maximum. Note that the supernova has not faded since the previous *J*-band image.

30 pixels and outer radius 40 pixels. We used the package PHOTCAL to calculate the transformation equations to determine zero points, color terms, and atmospheric extinction terms.

The color terms we obtained were actually very similar to the averaged transformations provided by ESO<sup>3</sup>. Since the ESO measurements are based on a larger number of standard stars, we decided to fix the color and extinction terms to the values determined by ESO.

This procedure allowed us to calibrate a number of local stars in the field of SN 2000cx. Photometry of the supernova

was then tied to the system of Landolt standards via these field stars, so that accurate supernova photometry could be established also on non-photometric nights.

To check the nightly zero points we also reduced the standard stars for the last epoch of observations. On that night we observed 3 standard fields with FORS1: PG2213-006, Rubin 152, and SA100-269, with a total of 9 useful standard stars (Landolt 1992). For the 14 local standard stars chosen all over the CCD frame, the magnitude differences between the first and last epochs had a root-mean-square (rms) of 0.015 mag in the *V* band. The largest difference, in the *B* band, was still less than 0.04 mag. The magnitudes for our local standards are given in Table 2, together with their offsets from the supernova. These magnitudes were measured in a 6-pixel radius aperture, and aperture corrected using the task MKAP. Errors in the aperture correction were typically less than 0.01 mag, but reached 0.016 mag in the *U* band. The magnitude errors for the standard stars reported in Table 2 are the photometric errors from PHOT added in quadrature to the rms difference in magnitude between the two epochs. The error budget for the local standards is certainly below 0.05 mag in all bands, possibly with the exception of the *U* band, which is always more difficult (e.g., Suntzeff 2000). The *U*-band uncertainties in Table 2 are simply the error estimates from PHOT, including errors for the transformations.

The supernova photometry was performed on each epoch in a 6-pixel radius aperture. The magnitudes for the supernova are given in Table 3. These magnitudes are aperture-corrected and tied to the Landolt standards via the local standards. Here we have estimated the supernova magnitudes as the mean value of the differential magnitudes compared to our 14 local standards as given in Table 2. The estimated uncertainties given in Table 3 are combined from the error estimate by PHOT and the standard deviation for the 14 different magnitude estimates for each filter and epoch. The latter error should to some extent also encapsulate uncertainties in aperture corrections, color transformations, and zero points.

## 2.2. Infrared observations

Near-infrared observations were obtained using the Infrared Spectrometer And Array Camera (ISAAC)<sup>4</sup> attached to UT1

<sup>3</sup> [www.eso.org/observing/dfo/quality/FORS2/qc/photcoeff/photcoeffs\\_fors2.html](http://www.eso.org/observing/dfo/quality/FORS2/qc/photcoeff/photcoeffs_fors2.html)

<sup>4</sup> <http://www.eso.org/instruments/isaac/>

of the ESO VLT. A log of the observations is given in Table 4, and regions of two images are displayed in Fig. 2.

We used the Short Wavelength (SW) imaging mode with the Rockwell Hawaii HgCdTe  $1024 \times 1024$  pixel array detector. The pixel size on the sky was  $0''.147$  and the field-of-view was  $2'.5 \times 2'.5$ . The observations were performed in the  $J$ ,  $H$ , and  $K_s$  bands in jitter mode, with small offsets performed between each image in order to allow for sky subtraction. As the supernova was positioned far out from the core of the galaxy, we did not have to dither separately for sky.

For the  $J$  band, the detector integration times (DITs) were 30 s, and each observation was built up from 3 DITs per exposure (NDITs). This means that we stayed on the same spot in the sky for  $\sim 1.5$  min. The number of exposures (NEXP) in each observational block was typically 15 in the  $J$  band, which gives total exposure times (NDIT $\times$ DIT $\times$ NEXP) of 1350 s per observing block in the  $J$  band. The exposure times for the other bands can be seen in Table 4. We performed  $K_s$  observations of SN 2000cx only for the first epoch, due to our limited amount of observing time.

The data were reduced with the Eclipse<sup>5</sup> and NOAO IRAF software. Dark and flatfield images were prepared using standard Eclipse recipes. The sky background level was subtracted and the images were summed using the routine `jitter` within Eclipse.

Photometric standard stars are observed regularly with ISAAC in service mode. We reduced the  $J$ ,  $H$ , and  $K_s$  images of S279-F (Persson et al. 1989) from our first epoch, as well as  $J$  and  $H$  images of S234-E (Persson et al. 1989), FS10, FS19, and FS32 (Hawarden et al. 2001) obtained on our last epoch of observations. From these images we measured the flux of the standard stars to establish zero points for the given night and passband. The average Paranal atmospheric extinction of  $0.11 \text{ mag airmass}^{-1}$  was used in the  $J$  band, as well as  $0.06$  and  $0.07 \text{ mag airmass}^{-1}$  in the  $H$  and  $K_s$  bands, respectively<sup>6</sup>.

In this way we were able to establish local standard stars in the field of SN 2000cx, although due to the smaller field of view of ISAAC, these were not the same stars as in the optical. The magnitudes of the local standard stars were measured using aperture photometry, and the magnitudes were aperture corrected using isolated and well-exposed stars. The magnitudes for the standard stars are shown in Table 5. The listed errors in  $J$  and  $H$  are the errors from PHOT and the rms magnitude difference between the two epochs added in quadrature. For the  $K_s$  band we have only listed errors from PHOT, since this band was used only at the first epoch. Thus, the somewhat smaller errors listed in this band are likely to be underestimated accordingly.

The magnitudes of the supernova were again measured using differential photometry, and the uncertainties estimated as rms errors from comparison with the 14 local standard stars, added in quadrature with the errors from PHOT. The supernova near-IR magnitudes are listed in Table 6. We note that

**Table 6.** Late-time near-IR magnitudes of SN 2000cx.

MJD <sup>a</sup>	Phase <sup>b</sup>	$J$	$H$	$K_s$
52 000+	(days)			
121.4	369	21.86 (0.08) <sup>c</sup>	21.33 (0.13)	20.32 (0.11)
173.3	421	21.83 (0.07)	21.05 (0.10)	
232.0	480	21.87 (0.09)	21.15 (0.14)	
233.0	481	21.73 (0.09)	20.95 (0.12)	
235.0	483	21.77 (0.11)	20.99 (0.11)	

<sup>a</sup> Refers to the first exposure.

<sup>b</sup> Days past maximum  $B$ -band light.

<sup>c</sup> Numbers in parentheses are uncertainties. However, as discussed in Sect. 2.2 the total IR uncertainties for the faint supernova are likely as large as  $0.15$  mag at these epochs.

**Table 7.** *HST* observations of SN 2000cx.

Date	Phase <sup>a</sup>	Filter	Magnitude	Exposure	PI
(UT)	(Days)			(s)	
2001 07 10	348	<i>F675W</i>	$21.98 \pm 0.06$	280	Filippenko
2001 07 10	348	<i>F814W</i>	$21.41 \pm 0.06$	280	Filippenko
2002 02 03	557	<i>F439W</i>	$24.38 \pm 0.25$	2100	Kirshner
2002 02 03	557	<i>F555W</i>	$24.32 \pm 0.08$	2100	Kirshner
2002 06 19	693	<i>F555W</i>	$25.20 \pm 0.17$	4200	Kirshner

<sup>a</sup> Days past  $B$ -band maximum light.

the supernova itself was fainter than most of our local standard stars at these late phases. This means that the error budget estimated by comparison with the standard stars is probably too optimistic. At these faint levels, sky subtraction errors in the near-IR are likely to dominate the errors. In fact, we verified our reductions by an independent estimate using the XDIMSUM package. However, by measuring ten sources close to the supernova, which all had magnitudes comparable to the supernova itself, we found a significant scatter in the estimated magnitudes between the different epochs. From this exercise, we instead estimate an error of  $\pm 0.15$  mag in the supernova near-IR magnitudes.

### 2.3. Late *HST* photometry

SN 2000cx was also observed with *HST*. A log of the *HST* observations is given in Table 7.

We retrieved the data from the *HST* science archive, which delivers the fully reduced WFPC2 images. The photometry was performed using the HSTPhot package as described by Dolphin (2000). This software fits point-spread functions (PSF) to the detected objects, and also accounts for charge transfer efficiencies and aperture corrections. Following Li et al. (2002), we used option 10 to measure the supernova magnitudes. This option uses local sky determination and default aperture corrections. The magnitudes in the WFPC system and error estimates from HSTPhot for SN 2000cx are also given in Table 7. An image of the supernova in the PC chip was presented by Li et al. (2002, their Fig. 1 bottom right). The supernova lies in a clean and isolated region, which ensures that aperture photometry in our high quality ground-based data is adequate for this object. We also do not see any signs of a light echo

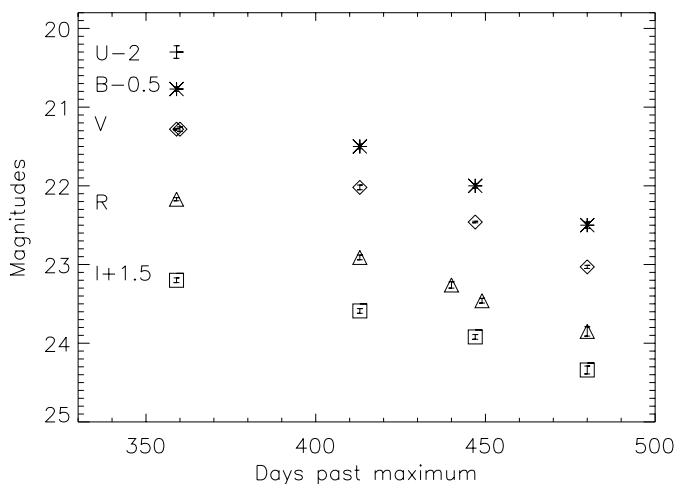
<sup>5</sup> <http://www.eso.org/projects/aot/eclipse/>

<sup>6</sup> [http://www.eso.org/instruments/isaac/imaging\\_standards.html](http://www.eso.org/instruments/isaac/imaging_standards.html)

**Table 8.** Decline rates in the VLT data<sup>a</sup>.

<i>B</i>	<i>V</i>	<i>R</i>	<i>I</i>	<i>J</i>	<i>H</i>
1.42 (0.04)	1.38 (0.01)	1.40 (0.03)	0.88 (0.04)	-0.06 (0.15)	-0.23 (0.15)

<sup>a</sup> Mag per 100 days between 360 and 480 days; errors in parenthesis are  $1\sigma$ .

**Fig. 3.** Late-time optical light curves of SN 2000cx; see Table 3. The magnitudes have been shifted for clarity as indicated.

(cf. Schmidt et al. 1994). No other star is detected close to the supernova position; moreover, the  $V - K$  and near-IR colors are not consistent with any stellar type, ruling out significant contamination from a foreground star in the late-time near-IR data.

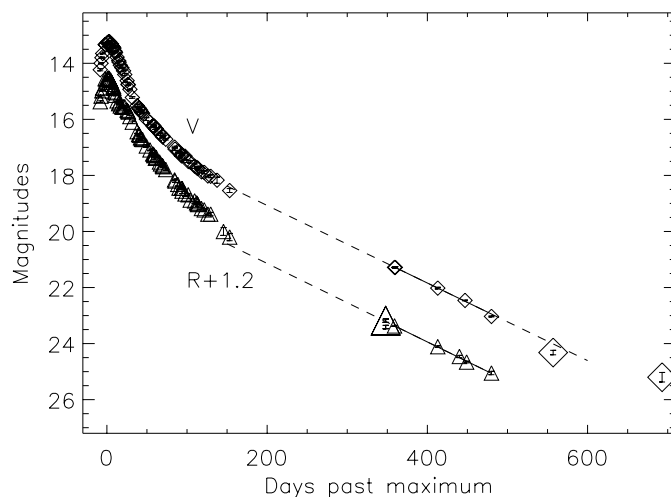
#### 2.4. Optical spectroscopy

At the first epoch of optical observations, 360 days past maximum, we also performed spectroscopy of SN 2000cx. On 24 July 2001 we obtained a 2400 s exposure using FORS2 on UT4. We used the 300V grism together with order-sorting filter GG375 and a  $1''3$  wide slit. Two nights later, on 26 July 2001, this was complemented by another 2400 s spectrum with the 300I grism and the OG590 filter. Together these two spectra cover the wavelength region  $\sim 3700$ – $9200$  Å.

The spectra were reduced in a standard way, including bias subtraction, flat fielding, and wavelength calibration using spectra of a Helium-Argon lamp. Flux calibration was done relative to the spectrophotometric standard star LTT377 with the 300V grism and to G158-100 with the 300I grism. The absolute flux calibration of the combined spectrum was obtained relative to our broad-band photometry.

### 3. Results

In Fig. 3 we plot the  $UBVRI$  photometry from our VLT observations. The flux from the supernova can be seen to decrease exponentially. A linear fit to the magnitudes gives the slopes presented in Table 8. The  $BVR$  light curves decline by about 1.4 mag per 100 days. This is consistent with the SNe Ia light curve slopes at earlier epochs (e.g., Turatto et al. 1990),

**Fig. 4.** The optical light curves of SN 2000cx. The early data are from Li et al. (2001). The  $R$ -band light curve has been shifted as indicated for clarity. The full lines are the best linear fits to the late-time VLT data, with slopes as given in Table 8. The dashed line is an extrapolation of this slope back to the early light curve. The late  $HST$  photometry is displayed with larger symbols. For the  $R$ -band point at 348 days past maximum, we have indicated the likely transformation from  $HST$  magnitudes to the  $R$ -band system (lower error bar).

and also reasonably consistent with the early light curve of SN 2000cx as published by Li et al. (2001). In Fig. 4 we plot the  $V$  and  $R$  light curves from that study, together with our late-time data. The dashed lines are the extrapolations of the late-time slopes to the early-time data. The  $I$  band, on the other hand, does not follow the other bands at late phases. At 0.88 mag per 100 days, this passband declines significantly more slowly.

The color evolution between 360 and 480 days past maximum is not very strong in the optical range. In Fig. 5 we show the  $B-V$ ,  $V-R$ , and  $R-I$  color evolution. Only in the  $R-I$  color can a clear trend be seen, due to the shallower slope in the  $I$ -band light curve.

The near-IR magnitudes from the VLT are plotted in Fig. 6. There is no evidence for any fading of the supernova flux during the observed epoch. This result is new and shows that substantial color evolution is indeed present at these very late phases. A linear fit to the  $JH$  light curves gives the decline rates presented in Table 8. The  $1\sigma$  errors on the decline rate were derived for a photometric error of  $\pm 0.15$  mag at each date.

Finally, also the very late-time observations with the  $HST$  have been added to the earlier light curves in Fig. 4. The earliest  $HST$  data, from day 348, have already been published by Li et al. (2002). They measured the WFPC2 magnitudes in the very same way as we have done, and with the same results (their Table 1). The magnitude we have plotted in the  $R$ -band

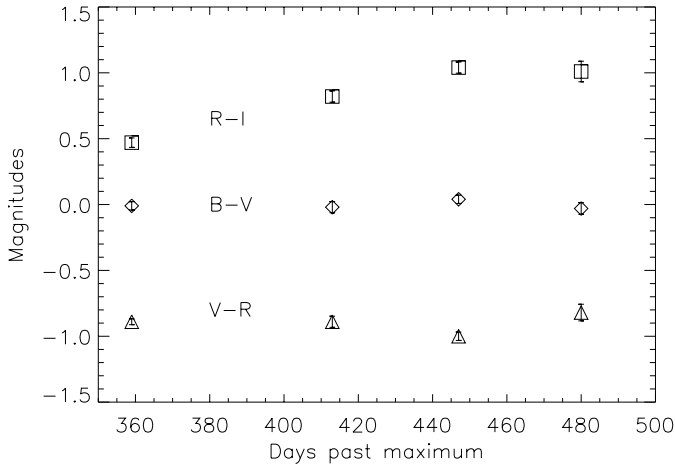


**Fig. 5.** Color curves for the late-time optical phases. There is little evolution in  $B - V$  and  $V - R$ , while  $R - I$  increases with time due to the slower decline rate in the  $I$  band.

light curve in Fig. 4 is the  $F675W$  magnitude, and should be converted to the Cousins  $R$ -band system. Li et al. (2002) obtained  $R = 22.14$  mag with a rough conversion using the transformation from Dolphin (2000)<sup>7</sup>. This is still consistent with our late light curve. In fact, as also noted by Li et al. (2002), the transformations used for converting magnitudes between these systems are not really applicable to emission-line objects. A better method may be to use our late-time spectrum obtained 360 days past maximum, to define the filter transformation. We used this spectrum, and integrated the flux under the filter functions for both the  $R$ -band filter and the  $HST F675W$  filter using the SYNPHOT task `p1trans`. This gave an offset of 0.23 (Vega) mag, which converts our measured  $F675W$  magnitude to  $R = 22.21$  mag, and similarly  $F814W$  to  $I = 21.68$  mag. Both transformations would make the  $HST$  magnitudes undershoot the light curves from the VLT, as illustrated by the added error bar in Fig. 4 for the transformed  $R$ -band magnitude at day 348. The later  $F555W$  magnitudes would accordingly have 0.15 mag added to convert to the  $V$  band. This is, however, under the assumption that the spectrum stays constant, and we have not taken this transformation into account in Fig. 4 or in the following discussion, where such an offset would not affect our conclusions in any way.

### 3.1. Bolometric luminosity

The wide  $UBVRIJHK$  coverage of our broad-band magnitudes allow an attempt to construct a UV-optical-IR (hereafter UVOIR) “bolometric” light curve. Such a light curve should represent the fraction of  $\gamma$ -ray and positron energy that is thermalized in the ejecta, although at these late phases some fraction of the energy is also escaping at even longer wavelengths.

To derive an absolute bolometric light curve we need the distance and reddening to SN 2000cx. The host extinction is expected to be small, since the supernova occurred in an

<sup>7</sup> Li et al. (2002) report  $R = 22.10$  mag from an approximation, but the more detailed calculation for these transformations gives  $R = 22.14$  mag.

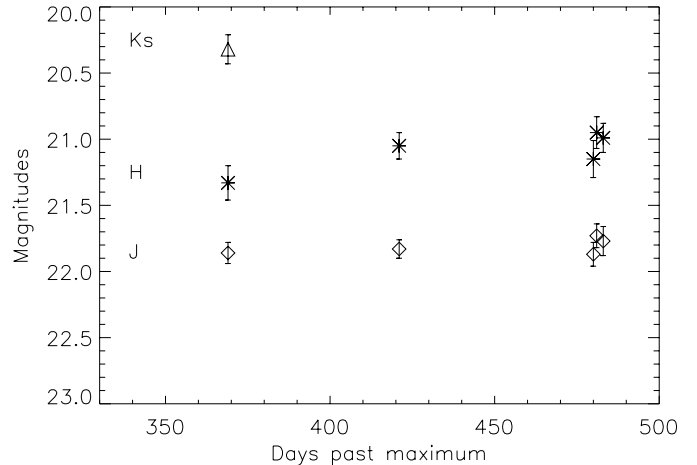


**Fig. 6.** Near-IR magnitudes and uncertainties (see Table 6) for SN 2000cx at late phases.

S0 galaxy, and far outside the central region. Early high-resolution spectra show no evidence for host galaxy Na I D absorption (Lundqvist et al. 2005). There is, however, a weak Galactic component of Na I D, consistent with the galactic reddening in the direction of SN 2000cx as derived by Schlegel et al. (1998),  $E(B - V) = 0.082$  mag. We will use this value for the total extinction toward SN 2000cx. The distance to SN 2000cx was reviewed in Candia et al. (2003) and is not very well constrained<sup>8</sup>. We will use a distance modulus of 32.47 mag in accordance with their analysis.

We made a simple UVOIR light curve in the following way. For the earlier epochs, we use the optical data ( $BVRI$ ) from Li et al. (2001), the near-IR data ( $JHK$ ) from Candia et al. (2003) and assume that  $U \approx B + 0.2$  (Candia et al. 2003, their Fig. 3). For our late VLT observations we assume that the  $U - B$  and  $H - K$  colors are constant during these epochs. We convert the magnitudes to flux using Fugutaki et al. (1995) and Allen (2000) for the optical and near-IR magnitudes, respectively. We then simply integrate the flux from  $U$  ( $0.36 \mu\text{m}$ ) to  $K$  ( $2.2 \mu\text{m}$ ) to form the UVOIR light curve. No assumptions are made on the fraction of emission lost outside this band (but see Suntzeff 1996). Where observations are missing, we simply interpolate. The extinction correction is done using the extinction law from Fitzpatrick (1999). The resulting light curve is displayed in Fig. 7.

## 4. Light curves of SNe Ia

There exist a rich literature regarding the light curves of SNe Ia (e.g., Leibundgut 2000, and references therein). Almost all such studies concern the early phases of the supernova, when it is bright and relatively easy to observe. The importance of these early phases has been greatly emphasized with the realization that SNe Ia can be used for accurate measurements of cosmological distances.

<sup>8</sup> The distance measurements to NGC 524 are actually quite dis-according. Surface Brightness Fluctuation measurements indicate a distance modulus of  $31.84 \pm 0.20$ , while a supernova estimate gives  $32.53 \pm 0.35$ .

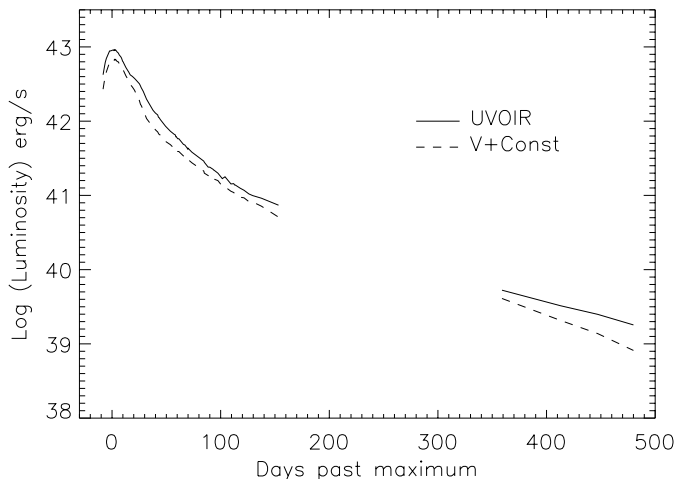


**Fig. 7.** UVOIR light curve for SN 2000cx. The early-epoch data are from Li et al. (2001, *(U)BVRI*) and Candia et al. (2003, *JHK*). The UVOIR curve is shown with the full line, while the dashed line is the V-band luminosity shifted arbitrarily along the ordinate. The details and assumptions for the construction of the UVOIR light curve are given in the text. The adopted distance is 31.2 Mpc.

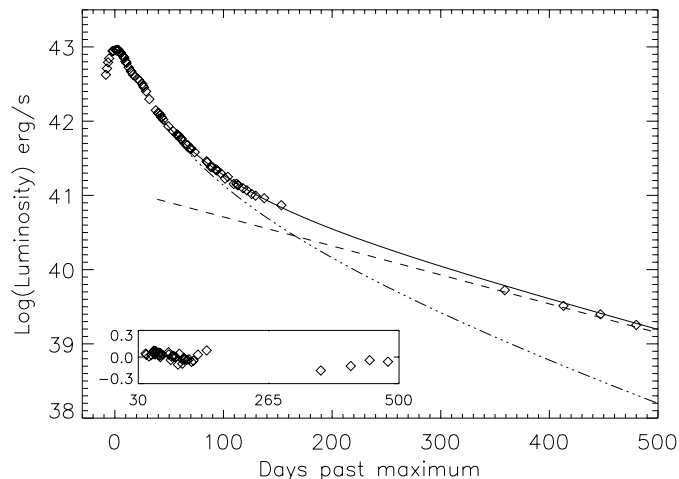


**Fig. 8.** Illustrative toy model of the bolometric luminosity for a SN Ia light curve powered by radioactivity. Diamonds show our UVOIR light curve for SN 2000cx. The full line is the total luminosity for a simple  $^{56}\text{Co}$  decay model (see text). Assuming  $0.28 M_{\odot}$  of  $^{56}\text{Ni}$ , the dot-dashed line shows the contribution from the  $\gamma$ -rays and the dashed line the contribution from the positrons. The inset shows the deviation in magnitudes versus time between the toy model and the data. The standard deviation is 0.05 mag.

The light curves of SNe Ia are powered by the deposition in the expanding SN ejecta of the  $\gamma$ -rays and positrons produced by the decay chain  $^{56}\text{Ni} \rightarrow ^{56}\text{Co} \rightarrow ^{56}\text{Fe}$ . The shape of the early-time light curve of a SN Ia depends essentially on the fact that optical photons created by the thermalization of the  $\gamma$ -rays and positrons do not immediately escape from the optically thick ejecta. Maximum light occurs when the instantaneous rates of deposition of hard radiation and emission of optical light are roughly equal (Arnett 1982). With time, the delay between energy deposition and emission of optical radiation becomes progressively smaller.

In this work we instead concentrate on the late phases. In the nebular phase, the ejecta are essentially optically thin. The light curves at these phases are still driven by the radioactive decay of  $^{56}\text{Co}$ , which decays on a timescale of 111.3 days. However, the few SNe Ia for which there exist well-monitored light curves at phases up to several hundred days decline substantially faster than this. Actually, such observations were available even before the understanding that  $^{56}\text{Co}$  powers the light curves, and early suggestions for the powering included nuclei with faster decay times, such as californium (Baade et al. 1956; see Colgate et al. 1997, for an interesting historical perspective). From nucleosynthesis arguments it was soon realized that most of the burned material is iron-group elements, and most importantly  $^{56}\text{Ni}$ . The observed rapid decline rate of the light curves is now instead interpreted in terms of escape of the  $\gamma$ -rays from the ejecta. As the ejecta expand, the optical depth decreases and a progressively larger fraction of the  $\gamma$ -rays escapes thermalization.

A simple toy model for the late emission can sometimes be instructive to understand the decay of a supernova light curve (e.g., Sollerman et al. 2002). In this model the flux from the decay of  $^{56}\text{Co}$  evolves as  $e^{-t/111.3} \times (1 - 0.966e^{-\tau})$ , where the optical depth,  $\tau = (t_1/t)^2$ , decreases due to the homologous expansion, and  $t_1$  sets the time when the optical depth to  $\gamma$ -rays

is unity. Furthermore, 3.4% of the energy in these decays is in the form of the kinetic energy of the positrons, which are here assumed to be fully trapped. Such a simplistic model can reasonably well fit the “bolometric” light curve of a SN Ia after the diffusion phase, with only two free parameters (Fig. 8).

As the  $\gamma$ -rays escape the ejecta, the relative importance of the positrons will increase, and as soon as the trapping of the  $\gamma$ -rays decreases to below 3.4% the light curve enters the positron-dominated phase. The shape of the bolometric light curve will then depend on whether or not the positrons are fully trapped. The simple model described above assumes full trapping, which is likely the case if the ejecta of SNe Ia have a strong and tangled magnetic field. In this case the light curve should flatten out and approach the decay time of  $^{56}\text{Co}$  in the positron-dominated phase (see Fig. 8). However, late-time observations of SNe Ia in optical passbands have indicated that the light curve continues to fall rapidly also at epochs later than 200 days.

This has been interpreted in two different ways. It could be that the positrons escape from the ejecta, and therefore cannot efficiently power the late-time light curve. Alternatively, more and more of the emission may emerge at longer wavelengths outside our observational coverage. To investigate these scenarios was the main motivation for our observational campaign of SN 2000cx.

The progressive transparency of positrons was suggested by Arnett (1979) and this positron escape scenario was elaborated by Colgate et al. (1980). It was observationally investigated by Cappellaro et al. (1997) and more recently by Milne et al. (1999, 2001), who suggested that positron escape must indeed occur in at least some SNe Ia in order to explain their late-time light curves. Ruiz-Lapuente & Spruit (1998) reached similar conclusions and connected them to the theory of the

white dwarf magnetic field. If positron escape is indeed needed to explain the rapidly declining late-time light curves, this implies weak or radially combed magnetic fields.

These comparisons between observations and simple models have, however, several caveats. Most importantly, the observations of late-time light curves are relatively sparse, and are available in a few passbands only. It is therefore not possible to construct true bolometric light curves. At earlier phases, attempts to construct UVOIR light curves for SNe Ia are indeed useful for comparisons to models (e.g., Contardo et al. 2000). At these phases, the UVOIR light curve embraces most of the emitted light (Suntzeff 1996; Contardo et al. 2000). This assumption is not necessarily valid at later phases, but has often been adopted due to the lack of detailed observations.

For example, the work of Cappellaro et al. (1997) simply assumed that the late *V*-band light curve follows the bolometric light curve at late phases. A similar assumption was made by Milne et al. (1999, 2001). However, we note that as the input heating decreases and the ejecta expand, the temperature is likely to decrease as well, and color evolution could then mimic the effect of positron escape.

To address this question requires comprehensive modeling of the nebular phase of the supernova. With a model that predicts where the emission will emerge, direct comparisons with filter-band curves can be made. The attempts to build a self-consistent model for a nebular SN Ia took off with the PhD thesis of Axelrod (1980). He argued against positron escape and instead suggested that the emission at late phases would emerge in the far-IR, thereby introducing the concept of the “infrared catastrophe”. This is a thermal instability that occurs when the temperature drops below what is needed to excite the optical atomic levels, and the cooling is abruptly taken over by the far-IR fine-structure lines.

To be able to interpret our observations of SN 2000cx, we have therefore constructed detailed models for the late phases of SNe Ia.

## 5. Modeling

We have modeled the emission from a SN Ia in the nebular phase, 100–1000 days after explosion. The adopted code is an updated version of the code described by Kozma & Fransson (1998a), and applied to SN 1987A by Kozma & Fransson (1998a,b). Below is a brief summary of the model.

### 5.1. The model

The supernova ejecta are powered by the decay of radioactive isotopes formed in the explosion. In the model we include the decays of  $^{56}\text{Ni}$ ,  $^{57}\text{Ni}$ , and  $^{44}\text{Ti}$ .  $^{56}\text{Ni}$  first decays to  $^{56}\text{Co}$  on a time scale of 8.8 days and then to stable  $^{56}\text{Fe}$  on a time scale of 111.26 days (all decay times are e-folding). In the decay of  $^{56}\text{Co}$  a fraction (3.4%) of the energy is released in the form of kinetic energy of the positrons.  $^{57}\text{Ni}$  decays rapidly (51.4 h) to  $^{57}\text{Co}$ , which then decays to stable  $^{57}\text{Fe}$  on a time scale of 391 days. The decay time scale of  $^{44}\text{Ti}$  is 87 years and this decay chain also includes emission of positrons. At the epochs

we are modeling, the decay of  $^{56}\text{Co}$  dominates the energy input. The  $\gamma$ -rays emitted in the decays scatter off free and bound electrons in the medium, and give rise to fast electrons (with an energy of  $\sim 0.01$ – $1$  MeV). These nonthermal electrons, as well as the positrons emitted in the decays, deposit their energy by heating, ionizing, or exciting the ejecta. The amount of energy going into these three different channels depends on the composition and degree of ionization and is calculated by solving the Boltzmann equation as formulated by Spencer & Fano (1954). Details of this calculation are given in Kozma & Fransson (1992). In our model the  $\gamma$ -ray and positron deposition is calculated for the different compositions and ionizations. We assume that the positrons are deposited locally, within the regions containing the newly synthesized iron.

As input to our calculations we use the density structure, abundances, and velocity structure from model W7 (Nomoto et al. 1984; Thielemann et al. 1986). The model is spherically symmetric containing zones of varying compositions. Also, the amounts of radioactive elements are taken from the W7 input model. We have made no attempts to alter the model to accomplish a better fit to the observations.

The temperature, ionization, and level populations in each zone are calculated time-dependently. We find that steady state is a good approximation up to  $\sim 500$  days. Thereafter, time dependence becomes increasingly important.

In addition to the atomic data given in Kozma & Fransson (1998a), the code has been updated to model SNe Ia. In particular we have extended and updated our treatment of the iron-peak elements. We have included charge transfer reactions between the iron ions (Liu et al. 1998) and extended the ionization balance for cobalt. For the iron ions we have updated the total recombination rates and added rates to individual levels (Nahar 1996, 1997a; Nahar et al. 1997b). In addition to the iron ions we solve Co II, Co III, Ni I, and Ni II as multilevel atoms.

### 5.2. Line transfer

For the line transfer we use the Sobolev approximation (Sobolev 1957, 1960; Castor 1970). The Sobolev approximation turns the line transfer into a purely local process: either the photon is re-absorbed on the spot or it escapes the medium. As the ejecta are expanding homologously, with a velocity much larger than the thermal velocity of the matter, this is a good approximation for an individual, well-separated line. However, especially in the UV, there are many overlapping lines, and one can expect UV scattering to be important. The effect of line scattering is to alter the emergent UV spectrum, but it also affects the UV field within the ejecta. The ionization of elements with low ionization potential is sensitive to the UV field (see Kozma & Fransson 1998a). During scattering the UV photons are shifted toward longer wavelengths, both due to a pure Doppler shift, but also because of the increased probability of splitting the UV photons into several photons of longer wavelengths. A more accurate treatment of the line scattering is therefore expected to decrease the importance of photoionization.

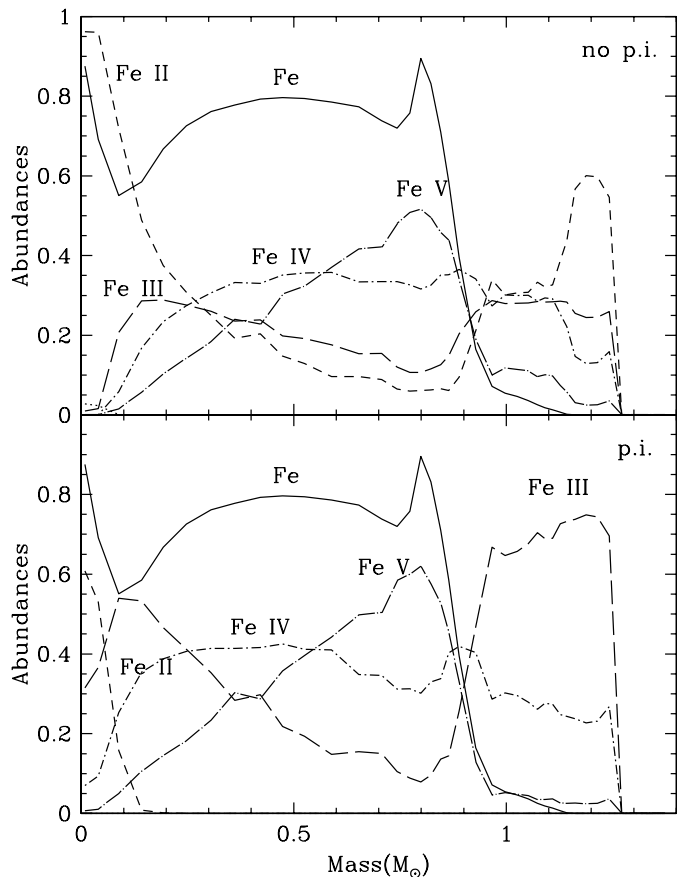


**Fig. 9.** Calculated ionization structure of iron in the supernova ejecta at 300 days for the two different models. The ionization for iron as a function of mass coordinate in the ejecta. The upper figure shows the result for the model without photoionization and the lower figure shows the result for the model including photoionization. The solid curve shows the total iron abundance. The broken curves show the fraction of the different iron ions.

To probe the effects of photoionization we have therefore made two model calculations, one without and the other including photoionization. These models to some extent represent the two extremes. The model including photoionization completely ignores the effects of UV scattering, while the model without photoionization assumes that all UV photons are redistributed to longer wavelengths. In the model including photoionization, we find that the ejecta are photoionized mainly by recombination emission. At 300 days the dominant contribution to the photoionization of Fe II is due to recombination to Fe III. The ionization structure of these models is displayed in Fig. 9, for the models both with and without photoionization included. This figure shows only the ionization for iron, which dominates the emission from SNe Ia at these late phases. The final output of the calculations is the detailed evolution of the emission of the ejecta at all wavelengths. Figure 10 shows the modeled and observed spectra of SN 2000cx at  $\sim 360$  days past maximum. Convolving the calculated spectra with the filter functions we also obtain passband light curves from the model. In Fig. 11 we show the light curves from this model, together with our late-time observations of SN 2000cx.

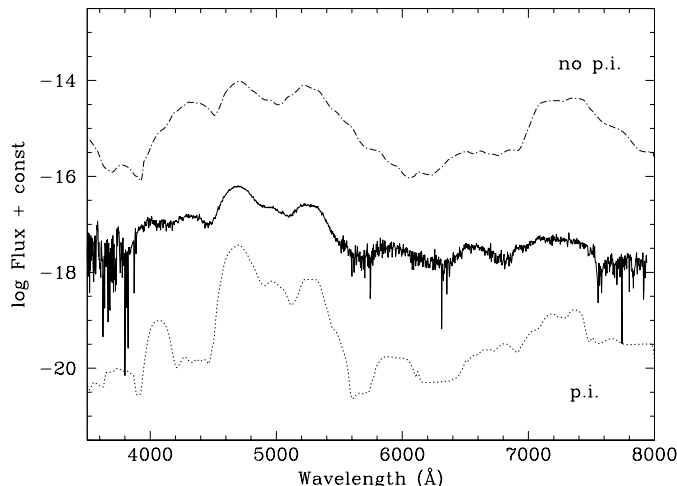


**Fig. 10.** Observed (*middle*) and modeled spectra of SN 2000cx at  $\sim 360$  days. The *upper* (dash-dotted) spectrum is a model calculation without photoionization, while the *lower* (dotted) spectrum is from a model including photoionization. The model spectra have been displaced by  $\pm 2$  dex, respectively. The most prominent feature is the emission between 4500 and 5500 Å. In the model including photoionization it is totally dominated by Fe III emission, while in the model without photoionization it is a mixture of Fe II and Fe III emission. The feature at 4700 Å is in this model mostly Fe III, while the emission at 5300 Å is dominated by Fe II. From the comparison between observed and modeled spectra we find somewhat better agreement for the model without photoionization.

## 6. Discussion

Although most SNe Ia are rather homogeneous in their properties, some are quite different. SN 2000cx was clearly photometrically peculiar at early phases (Li et al. 2001). It provided a bad fit to standard supernova light curves around maximum light, and showed anomalously blue colors after maximum. It is not at all clear, however, how the early appearance correlates with the later phases. It has recently been suggested that the peculiarities at early phases were related to a fast-moving clump just outside the supernova photosphere (Branch et al. 2004). This is unlikely to affect the emission at later phases. Here we use our late-time observations of SN 2000cx for a general discussion of the late-time emission from SNe Ia. We also note that our modeling is totally generic, and in no way adapted to fit this particular supernova. Instead of adjusting input parameters to improve the fits to the data, we will use the models for a general discussion. In Fig. 12 we also compare the V-band light curve of SN 2000cx with the light curve of another well-observed SN Ia, SN 1992A, and show that the late-time behavior of SN 2000cx is not very different. A future larger sample of SN Ia late-time light curves, in particular in the near-IR, is nevertheless needed to assess the applicability of SN 2000cx for a general discussion.

### 6.1. The importance of near-IR light curves

The main result of these observations is the constant emission in the near-IR during the observed epochs (Fig. 6). We are not aware of other such systematic observation of a late-time

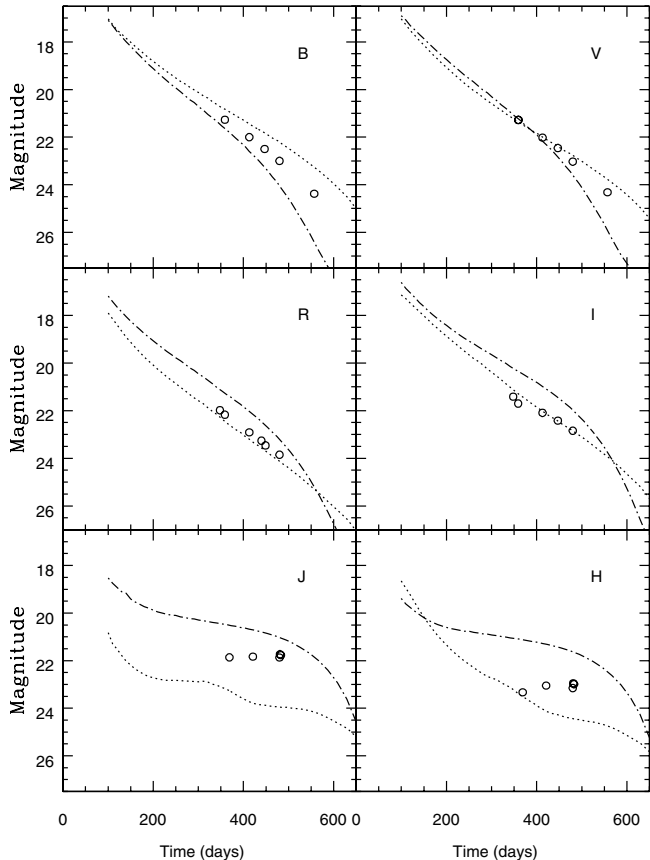


**Fig. 11.** Light curves for the *B* to *H* bands. The open circles are our observations obtained with the VLT and *HST*. Two models are shown, one including photoionization (dotted curve), and the other without photoionization (dash-dotted curve).

near-IR light curve of a SN Ia. In fact, very little has been published in this respect since the sparse, but pioneering, observations presented by Elias & Frogel (1983). Recently, two late-time *H*-band data points for SN 1998bu (250–350 days past maximum) suggest that this SN Ia also had a flat near-IR light curve at late phases (Spyromilio et al. 2004).

Our constant *J*-band and *H*-band light curves immediately highlight the main point of our study, the increasing importance of the near-IR at late phases. From our constructed UVOIR light curve, we can investigate where most of the energy emerges. In Fig. 13 we show the fraction of energy in the near-IR bands compared to the UVOIR luminosity as it evolves with time. This color evolution is also seen in Fig. 7 where the UVOIR light curve is plotted together with the (arbitrarily shifted) *V*-band light curve. While the *V* band follows the UVOIR light curve reasonably well at early phases, at the later epochs the *V* band declines faster than the UVOIR curve.

The increasing importance of the near-IR can also be seen in our detailed modeling. In Fig. 11 the light curves for the *B* band through *H*-band are shown for both observations and models. We find generally good agreement between observations and models, with a steeper slope in the *B*, *V*, *R*, and *I* bands, and almost constant light curves in the *J* and *H* bands. The almost constant emission in the near-IR bands is due to a shift of emission from iron lines in the optical to the strong

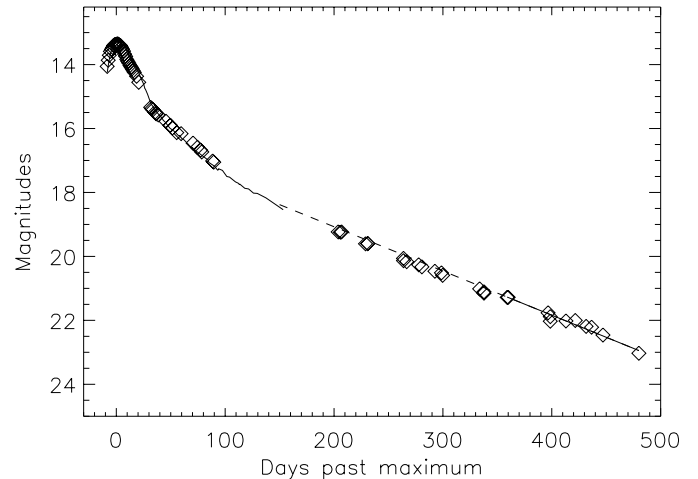


**Fig. 12.** SN 2000cx in the *V* band (full line, see also Fig. 4) compared to SN 1992A (diamonds; Suntzeff 1996). The magnitude and date of maximum for SN 1992A have been matched to the light curve of SN 2000cx. There is no indication that SN 2000cx behaves in a different way than SN 1992A at late phases. SN 1992A had a very normal late-time light curve (e.g., Fig. 2 in Leibundgut 2000).

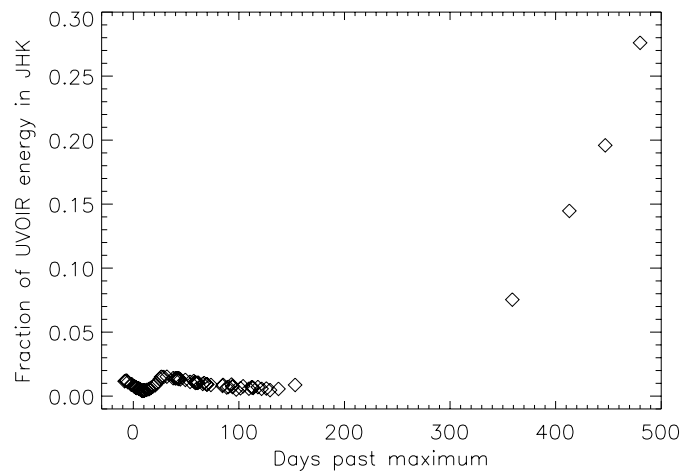


**Fig. 13.** Fraction of the luminosity in the near-IR bands as a function of time. The fraction is the luminosity in the near-IR bands divided with the total UVOIR luminosity ( $L_{JHK}/L_{UBVRIJHK}$ ), where the UVOIR light curve has been constructed as described in Sect. 3.1.

near-IR [Fe II] lines, which dominate the *J* and *H* bands. In this way, the temperature decrease in the ejecta gives a color evolution momentarily compensating the decreasing radioactive input in the near-IR bands.

While our observations only cover the UVOIR range, the models naturally incorporate the true bolometric light curves. Figure 14 shows a comparison of this bolometric light curve and the *V*-band light curve. Here we can clearly see that the *V* band does not follow the bolometric light curve at the epochs of our observations. For the model without photoionization the *V* band drops rapidly around 400–500 days, while for the photoionization model the drop is significantly less rapid. The evolution in the *V* band reflects the temperature and ionization evolution of the ejecta. The temperatures in the model with photoionization are higher, and therefore a larger fraction of

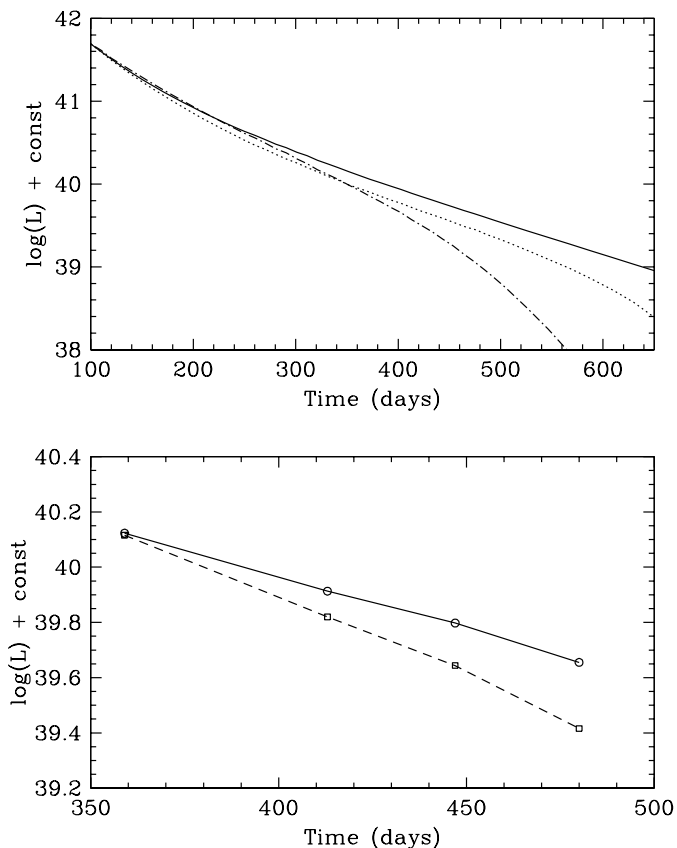


**Fig. 14.** Calculated (*upper panel*) and observed (*lower panel*) light curves for SN 2000cx. The solid line in the upper panel shows the bolometric luminosity, and the other lines show *V*-band luminosities for our two models. The dotted curve refers to the model including photoionization, and the dash-dotted curve refers to the model without photoionization. The lower panel shows results from the observations. The solid curve is the integrated luminosity in the *UBVRIJHK* bands, while the dashed curve is the luminosity in the *V* band. The *V*-band curves are vertically shifted in both panels.

the luminosity is emerging in the *V* band. For the model without photoionization the emission is emerging at longer wavelengths. The lower panel of Fig. 14 shows the observed UVOIR light curve compared with the observed *V*-band light curve (i.e., this is basically a close-up of the late phases shown in Fig. 7). The implications are further discussed below.

## 6.2. The nickel mass

The simple toy model adopted for the light curve in Fig. 8 provides a reasonable fit to the UVOIR light curve. This exercise reveals several potentially interesting aspects of the light curve.

We note that the slope of the four late epochs in the UVOIR light curve is  $\sim 1.0$  mag per 100 days. Intriguingly, this is the same as the decay time scale of  $^{56}\text{Co}$  and in the simple model the good match is solely due to powering of the kinetic energy of completely trapped positrons (dashed curve, Fig. 8). If this interpretation is valid, and if the UVOIR light curve describes the true bolometric luminosity of the supernova at these epochs, the nickel mass can be directly

deduced. The toy model light curve in Fig. 8 is from  $L = 1.3 \times 10^{43} M_{\text{Ni}} e^{-t/111.3} (1 - 0.966e^{-\tau})$ , in units of  $\text{erg s}^{-1}$ , where  $M_{\text{Ni}}$  is the amount of  $^{56}\text{Ni}$  in solar masses and the other parameters are as defined in Sect. 4 above. For this simple scenario, only including  $^{56}\text{Co}$ , the parameter  $t_1$  is related to the time when positrons start to dominate ( $t_{\text{pos}}$ ) by  $t_{\text{pos}} = 5.27 t_1$ . In a least-squares sense, the best fit is for a nickel mass of  $0.28 M_{\odot}$  and  $t_1 = 31.5$  days (fitting all data later than day 50).

Two ways to derive nickel masses from the photometry of SNe Ia have been employed (see, e.g., Leibundgut & Suntzeff 2003, for a review). Cappellaro et al. (1997) adopted a simple light-curve model for the late epochs of the supernova light curve and used the *V* band as a surrogate for the bolometric luminosity. This is in a way similar to the discussion above, but we have already noted that at these late phases it is not correct to assume the *V* band to closely follow the bolometric light curve.

The standard way to derive a nickel mass has rather been to use the peak luminosity. According to Arnett's rule (Arnett 1982; Pinto & Eastman 2000), the luminosity at the peak directly reflects the input powering from the radioactivity. This has been used by Contardo et al. (2000) and others to derive nickel masses for a number of SNe Ia. The main uncertainty is usually the poorly known distances and extinctions to the supernovae.

Using the formalism of Contardo et al., the peak UVOIR luminosity in Fig. 8 corresponds to  $\sim 0.46 M_{\odot}$  of  $^{56}\text{Ni}$ . In fact, since we have omitted any flux outside the  $0.36\text{--}2.2 \mu\text{m}$  range, the actual peak luminosity must be somewhat higher (Candia et al. 2003; Suntzeff 1996)<sup>9</sup>.

We derive a smaller nickel mass from the late phases compared to the peak, given the same distance modulus and extinction. This is likely due to the fact that at these late phases, even the UVOIR light curve does not encapsulate the total bolometric luminosity. If so, this can then be used to derive the fraction of emission outside the covered bands. We thus see that our observations indicate that at 500 days about 40% of the emission is emerging outside our observed range, most likely redward of the *K* band.

This agrees reasonably well with our detailed models, where we can see that only about 75% of the emission at 400 days is in the UVOIR wavelength range, while the mid-IR and far-IR include most of the remaining power. Adjusting the derived nickel mass for this recovers  $\sim 0.4 M_{\odot}$  of  $^{56}\text{Ni}$ .

The late-time UVOIR slope points to complete (or at least constant) trapping of positrons, and gives no hint of temporal color evolution out of the observed bands. The models do in fact show a slow evolution, in that the UVOIR range progressively lose energy to the far-IR, but this is also one of the aspects where the model is clearly not completely correct (see Sect. 6.3).

<sup>9</sup> The peak luminosity of SN 2000cx from Candia et al. (2003),  $\log(L/\text{erg s}^{-1}) \approx 43.05$ , corresponds according to Contardo et al. (2000) to  $\sim 0.56 M_{\odot}$ , but Contardo et al. also did not include the UV part of the spectrum. The actual nickel mass of course depends crucially on the assumed distance, which is rather uncertain; we adopt 31.2 Mpc.

In our models we have used a nickel mass of  $0.6 M_{\odot}$  from the W7 model, and the same distance modulus and reddening as adopted for SN 2000cx. However, the fits to the data in Fig. 11 are not really good enough to determine the nickel mass with any precision. A lower nickel mass would clearly enhance the rapid luminosity drop, but this is also affected by the density (i.e., the assumed ejecta mass and expansion velocity).

### 6.3. The IR catastrophe

The significance of a thermal instability for SNe Ia at late phases was recognized by Axelrod (1980). At low temperatures the cooling of the ejecta is rapidly shifted from the optical into the IR fine-structure lines (e.g., [Fe I]  $24 \mu\text{m}$ , [Fe II]  $26 \mu\text{m}$ ). This so-called “infrared catastrophe” would drastically decrease the flux in the optical. Fransson et al. (1996) also found a rapid decrease in the optical flux at  $\sim 500$  days past explosion in their modeling, and realized that this was not in accordance with late-time optical observations of SN 1972E. Now, 10 years later, the accuracy of the atomic data needed for these models, as well as the computing facilities, have improved significantly. Still, our new models show the same effect.

In Fig. 11 it can be seen that the curves for the model without photoionization drops quickly after 400–600 days. The faster drop in this model is due to a lower temperature in the ejecta. Again, this rapid drop in flux is in conflict with the late-time observations (in particular the very last epoch). Since these models attempt to include our best knowledge of the physics of the emission of the supernova, the reason for this discrepancy is important to understand.

When looking at the ionization structure for the two models at 300 days (Fig. 9), we find that the degree of ionization is significantly higher in the photoionization model. Especially in the outermost region (where the iron abundance is small) the amount of Fe III, at the expense of Fe II, increases when the photoionization is turned on. It is the recombination emission (to Fe III) from the underlying regions that photoionizes Fe II. In both models the amount of Fe I is negligible at this epoch. In fact, although our spectral calculations based on these ionization structures give a decent fit to the observed spectrum (Fig. 10), it appears as if the model with lower ionization does the best job. The light curve models in Fig. 11 do instead favor the models including photoionization. A proper treatment of the UV scattering is thus clearly important, but since the differences in the light-curve slopes are mainly a temperature effect there are other scenarios which might provide similar results. To avoid the IR catastrophe there is basically a need to keep the ejecta warmer than a critical temperature where this instability sets in. This can be obtained in several ways. For example, a higher nickel mass would give higher temperature and ionization. Another possible mechanism is clumping of the ejecta, which would give regions of lower and higher densities, and the low-density regions would be hotter due to less efficient cooling. Yet another scenario which would affect the temperature structure in the ejecta is the non-local deposition of positrons. These matters are beyond the scope of the current investigation and will be discussed elsewhere.

### 6.4. Positron escape

The above results demonstrate the difficulty in interpreting supernova light curves for which observations only exist over a limited wavelength range.

Milne et al. (2001) used a Monte Carlo scheme to simulate the deposition of  $\gamma$ -rays and positrons in the ejecta. They claim that late light curves of SNe Ia can be reproduced only if a substantial fraction of the positrons escape from the ejecta. They based that claim upon the suggestion that at late phases ( $\geq 40$  days), the  $V$  band constitutes a constant ( $\sim 25\%$ ) fraction of the 3500–9700 Å emission, which they loosely referred to as the bolometric luminosity. We show that by including UVOIR photometry in the determination of a bolometric luminosity, at late phases the  $V$  band is seen to deviate from the bolometric luminosity for SN 2000cx.

In Fig. 14 we compare the bolometric light curve to the  $V$ -band light curve for our model calculations and observations. These model calculations assume instant and local deposition of the positrons. Even in this case of full positron trapping we find an increasing deviation between the bolometric and  $V$ -band light curve with time. The lower panel of Fig. 14 shows our observations, where we also find that the slope of the bolometric and  $V$ -band light curves differs. A comparison to a true bolometric light curve would further increase this effect.

It is clear that this shift of the emission into the IR passbands with time will mimic the effect of positron escape. Deviations between simple models and the  $V$ -band light curve should therefore not be interpreted in terms of the degree of positron escape. Instead, a detailed and consistent knowledge of the temperature and ionization evolution of the ejecta is required. This means that many previous studies of positron escape from the late-time ejecta in SNe Ia in fact require more detailed observations and modeling than hitherto appreciated to draw definitive conclusions on positron trapping.

### 6.5. The very late-time light curve

Lastly, we note that the  $V$ -band decline appears to level out in the two final *HST* observations; the slope is only 0.65 mag per 100 days between day 557 and 693 in the  $F555W$  *HST* observations. It is hazardous to draw any general conclusions from a single passband since there are many ways to power the late-time light curve of a supernova (see, e.g., Sollerman et al. 2002). This section is therefore rather speculative.

First of all, there could of course be a late-time light echo, as seen for SN 1998bu. However, the SO host galaxy should be clear of dust and the *HST* images show no evidence for a ring. We note also that the SN Ia 1992A displayed a slow  $F555W$  evolution at these late phases (Cappellaro et al. 1997). This behavior may thus be generic for thermonuclear supernovae.

The final bright  $V$ -band observation immediately shows that the IR catastrophe as indicated in the models does not occur at these phases. As noted previously, there are many possible solutions to this dilemma.

Potentially,  $^{44}\text{Ti}$  could become important at late phases, since it decays on a time scale of 87 years, and the decay mainly

results in positrons. However, to influence the light curve at our last epoch of observations requires a large abundance of titanium – as much as 7% of the original mass of  $^{56}\text{Ni}$ . This is much more than in the W7 model, which we have used for our detailed calculations, and is likely ruled out from nucleosynthesis arguments at the temperatures reached in SN Ia burning fronts.

We emphasize that this late observation is only in the  $V$  band, and is not representing the bolometric luminosity. Thus, any effect that could boost the emission in this band relative to the other bands would give a shallower slope in the  $V$  band. In our model calculations we find that after  $\sim 650/800$  days (without/with photoionization) Fe I dominates the emission in the  $V$  band. Fe I emits relatively more in the  $V$  band and this results in a flattening of the  $V$ -band light curve (see also Fransson et al. 1996). However, even though our modeled slope of the  $V$ -band light curve levels out, the total flux of Fe I is clearly too low compared to the observations. Also, the epoch at which Fe I starts to dominate is too late. A model with a clumpy medium could possibly overcome these problems. Another possible effect is indeed a longer lifetime of the positrons that allows time-dependent effects to become dominant. This is very speculative and more very late-time observations of SNe Ia are needed before any serious discussion can be made.

## 7. Summary

We have conducted a systematic and comprehensive monitoring programme of the SN Ia 2000cx at late phases using the VLT and *HST*. The VLT observations cover phases 360 to 480 days past maximum and includes photometry in the  $(U)BVRIJH(K)$  bands. While the optical bands decay by about 1.4 mag per 100 days, we find that the near-IR magnitudes stay virtually constant during the observed period. This means that the importance of the near-IR to the bolometric light curve increases with time. The finding is also in agreement with our detailed modeling of a SN Ia in the nebular phase. In these models, the increased contribution of the near-IR is simply a temperature effect. We note that this complicates late-time studies where often only the  $V$  band is well monitored. In particular, it is not correct to assume that any optical band follows the bolometric light curve at these phases, and any conclusions based on such assumptions must be regarded as premature.

We have found that a very simple model where all positrons are trapped can reasonably well account for the UVOIR observations. The nickel mass deduced from the positron tail of this light curve is lower than found from the peak brightness, which provides the fraction of emission outside the observed range at the late phases. Our detailed models show the signature of an infrared catastrophe at these epochs, which is not supported by the observations. More importantly, at the observed epochs, the gradual lowering in temperature increases the importance of the near-infrared emission. These conclusions are drawn from observations of a single supernova, which was clearly unusual at the peak. We support this generalization by detailed modeling and comparisons to the late-time light curve of SN 1992A. It is clear, however, that these suggestions have to be verified

by more data of thermonuclear supernovae at very late phases. Such a programme is currently ongoing. The investigation of positron escape from SNe Ia thus awaits observations that better represent the bolometric luminosity as well as more realistic models.

*Acknowledgements.* We are grateful to Ken Nomoto for providing the W7 model, and to Sultana Nahar for providing recombination rates for the iron ions. We also thank Nick Suntzeff for important input in the early phases of this project. We thank the ESO VLT staff for their assistance with the observations. A.V.F. is grateful for NSF grants AST-9987438 and AST-0307894, as well as for NASA grants GO-8602 and GO-9114 from the Space Telescope Science Institute (STScI), which is operated by AURA, Inc., under NASA contract NAS 5-26555.

## References

- Allen, C. W. 2000, *Allen's Astrophysical Quantities*, 4th edition, ed. A. N. Cox
- Arnett, W. D. 1979, *ApJ*, 230, 37
- Arnett, W. D. 1982, *ApJ*, 253, 785
- Axelrod, T. C. 1980, Ph.D. Thesis, University of California, Santa Cruz
- Baade, W., Burbidge, G. R., Hoyle, F., et al. 1956, *PASP*, 68, 296
- Branch, D., Thomas, R. C., Baron, E., et al. 2004, *ApJ*, 606, 413
- Candia, P., Krisciunas, K., Suntzeff, N. B., et al. 2003, *PASP*, 115, 277
- Castor, J. I. 1970, *MNRAS*, 149, 111
- Chornock, R., Leonard, D. C., Filippenko, A. V., et al. 2000, *IAUC*, 7463
- Colgate, S. A., Petscheck, A. G., & Kriese, J. T. 1980, *ApJ*, 237, L81
- Colgate, S., Fryer, C., & Hand, K. P. 1997, in *Thermonuclear Supernovae*, ed. P. Ruiz-Lapuente, R. Canal, & J. Isern (Dordrecht: Kluwer), 273
- Contardo, G., Leibundgut, B., & Vacca, W. D. 2000, *A&A*, 359, 876
- Dolphin, A. E. 2000, *PASP*, 112, 1383
- Elias, J. H., & Frogel, J. A. 1983, *ApJ*, 268, 718
- Filippenko, A. V. 1997, *ARA&A*, 35, 309
- Fitzpatrick, E. L. 1999, *PASP*, 111, 63
- Fransson, C., Houck, J., & Kozma, C. 1996, in *Supernovae and supernova remnants*, ed. R. McCray, & Z. Wang (Cambridge: Cambridge Univ. Press), IAU Coll., 145, 211
- Fukugita, M., Shimasaku, K., & Ichikawa, T. 1995, *PASP*, 107, 945
- Hawarden, T. G., Leggett, S. K., Letawsky, M. B., Ballantyne, D. R., & Casali, M. M. 2001, *MNRAS*, 325, 563
- Hoyle, F., & Fowler, W. A. 1960, *ApJ*, 132, 565
- Kozma, C., & Fransson, C. 1992, *ApJ*, 390, 602
- Kozma, C., & Fransson, C. 1998a, *ApJ*, 496, 946
- Kozma, C., & Fransson, C. 1998b, *ApJ*, 497, 431
- Landolt, A. 1992, *AJ*, 104, 340
- Leibundgut, B. 2000, *A&ARv*, 10, 179
- Leibundgut, B., & Suntzeff, N. B. 2003, in *Supernovae and Gamma-Ray Bursters*, ed. K. Weiler (New York: Springer), 77
- Li, W., Filippenko, A. V., Gates, E., et al. 2001, *PASP*, 113, 1178
- Li, W., Filippenko, A. V., Van Dyk, S., et al. 2002, *PASP*, 114, 403
- Liu, W., Jeffery, D. J., & Schultz, D. R. 1998, *ApJ*, 494, 812
- Lundqvist, P., Sollerman, J., Mattila, S., et al. 2005, in preparation
- Mazzali, P., Nomoto, K., Cappellaro, E., et al. 2001, *ApJ*, 547, 988
- Milne, P. A., The, L. S., & Leising, D. 1999, *ApJS*, 124, 503
- Milne, P. A., The, L. S., & Leising, D. 2001, *ApJ*, 559, 1019
- Nahar, S. N. 1996, *Phys. Rev. A*, 53, 2417
- Nahar, S. N. 1997, *Phys. Rev. A*, 55, 1980
- Nahar, S. N., Bautista, M. A., & Pradhan, A. K. 1997, *ApJ*, 479, 497

- Nomoto, K., Thielemann, F.-K., & Yokoi, K. 1984, *ApJ*, 286, 644
- Perlmutter, S., Aldering, G., Goldhaber, G., et al. 1999, *ApJ*, 517, 565
- Persson, S. E., Murphy, D. C., Krzeminski, W., Roth, M., & Rieke, M. J. 1998, *AJ*, 116, 2475
- Pinto, P., & Eastman, R. 2000, *ApJ*, 530, 757
- Riess, A. G., Filippenko, A. V., Challis, P., et al. 1998, *AJ*, 116, 1009
- Ruiz-Lapuente, P., & Spruit, H. 1998, *ApJ*, 500, 360
- Schlegel, D. J., Finkbeiner, D. P., & Davis, M. 1998, *ApJ*, 500, 525
- Schmidt, B. P., Suntzeff, N. B., Phillips, M. M., et al. 1994, *ApJ*, 434, 19
- Schmidt, B. P., Kirshner, R. P., Leibundgut, B., et al. 1998, *ApJ*, 507, 46
- Sobolev, V. 1957, *SvA*, 1, 678
- Sobolev, V. 1960, *Moving Envelope of Stars* (Cambridge: Harvard Univ. Press)
- Sollerman, J., Holland, S. T., Challis, P., et al. 2002, *A&A*, 386, 944
- Sollerman, J., Kozma, C., & Lindahl, J. 2004, in *Proc. IAU*, 192 [arXiv:astro-ph/0311075]
- Spencer, L. V., & Fano, U. 1954, *Phys. Rev.*, 93, 1172
- Spyromilio, J., Gilmozzi, R., Sollerman, J., et al. 2004, *A&A*, 426, 547
- Suntzeff, N. B. 2000, in *Cosmic Explosions*, ed. S. S. Holt, & W. W. Zhang (New York: American Inst. of Physics), 65
- Suntzeff, N. B. 1996, in *Supernovae and supernova remnants*, ed. R. McCray, & Z. Wang (Cambridge: Cambridge Univ. Press), IAU Coll., 145, 41
- Thielemann, F.-K., Nomoto, K., & Yokoi, K. 1986, *A&A*, 158, 17
- Turatto, M., Cappellaro, E., Barbon, R., et al. 1990, *AJ*, 100, 771
- Yu, C., Modjaz, M., & Li, W. 2000, *IAUC*, 7458

# Online Material

**Table 1.** Log of optical VLT observations, SN 2000cx.

Date (UT)	Filter	MJD <sup>a</sup>	Exposure (s)	Airmass <sup>a</sup>	Seeing (arcsec)
2001 07 21	<i>B</i>	52 111.36	2 × 300	1.31	1.05
2001 07 21	<i>V</i>	52 111.37	2 × 240	1.29	0.98
2001 07 21	<i>R</i>	52 111.38	2 × 240	1.27	0.91
2001 07 21	<i>I</i>	52 111.38	2 × 500	1.25	0.90
2001 07 21	<i>U</i>	52 111.40	2 × 780	1.23	1.05
2001 07 22	<i>V</i>	52 112.34	2 × 300	1.38	0.91
2001 09 13	<i>V</i>	52 165.25	3 × 300	1.23	0.94
2001 09 13	<i>I</i>	52 165.26	3 × 800	1.22	0.86
2001 09 13	<i>B</i>	52 165.29	3 × 400	1.21	0.92
2001 09 13	<i>R</i>	52 165.31	4 × 400	1.23	0.87
2001 10 10	<i>R</i>	52 192.13	750+418	1.34	0.93
2001 10 17	<i>I</i>	52 199.15	8 × 650	1.24	0.68
2001 10 17	<i>B</i>	52 199.22	4 × 750	1.24	0.67
2001 10 17	<i>V</i>	52 199.25	4 × 750	1.35	0.86
2001 10 19	<i>R</i>	52 201.22	4 × 750	1.25	0.86
2001 11 19	<i>I</i>	52 232.02	8 × 650	1.38	0.92
2001 11 19	<i>R</i>	52 232.08	4 × 750	1.21	0.78
2001 11 20	<i>V</i>	52 233.02	4 × 750	1.36	0.84
2001 11 20	<i>B</i>	52 233.06	4 × 750	1.24	0.79

<sup>a</sup> Refers to the first exposure.

**Table 2.** Magnitudes for local standards in the optical

Offsets <sup>a</sup>		<i>U</i>	<i>B</i>	<i>V</i>	<i>R</i>	<i>I</i>
115.12 W	17.86 N	23.69 (0.18) <sup>b</sup>	23.29 (0.04)	22.45 (0.02)	22.00 (0.01)	21.48 (0.02)
134.48 E	154.34 S	21.59 (0.03)	21.54 (0.03)	20.77 (0.02)	20.29 (0.01)	19.76 (0.01)
140.48 E	88.12 S	24.16 (0.20)	23.04 (0.03)	21.48 (0.02)	20.58 (0.01)	19.55 (0.01)
52.08 W	116.12 S	22.59 (0.06)	21.94 (0.02)	20.86 (0.02)	20.23 (0.01)	19.57 (0.01)
40.55 W	106.03 S	22.73 (0.07)	22.62 (0.04)	21.80 (0.01)	21.30 (0.01)	20.73 (0.02)
158.45 E	45.25 N	22.40 (0.07)	23.17 (0.04)	22.38 (0.01)	21.84 (0.02)	21.29 (0.03)
156.22 E	187.75 N	21.52 (0.03)	21.68 (0.01)	21.18 (0.02)	20.85 (0.02)	20.47 (0.01)
188.73 E	6.06 S	24.13 (0.22)	23.04 (0.02)	21.60 (0.02)	20.72 (0.02)	19.67 (0.01)
24.84 W	12.28 N	24.51 (0.29)	23.59 (0.03)	22.69 (0.03)	22.15 (0.02)	21.49 (0.02)
62.29 W	9.51 N	24.55 (0.28)	23.88 (0.04)	22.97 (0.03)	22.45 (0.02)	21.83 (0.03)
68.48 W	121.36 S	23.01 (0.10)	23.09 (0.02)	22.15 (0.02)	21.60 (0.01)	20.95 (0.01)
109.51 W	180.10 N	23.77 (0.15)	23.57 (0.03)	22.86 (0.03)	22.39 (0.02)	21.86 (0.02)
88.22 W	78.11 S	23.02 (0.09)	23.08 (0.02)	22.34 (0.02)	21.88 (0.02)	21.32 (0.02)
82.48 E	104.51 S	23.86 (0.18)	24.05 (0.04)	22.92 (0.03)	22.01 (0.02)	21.18 (0.02)

<sup>a</sup> Offsets in arcseconds measured from the supernova.<sup>b</sup> Numbers in parentheses are uncertainties.

**Table 4.** Log of near-IR observations, SN 2000cx.

Date (UT)	Filter	MJD <sup>a</sup>	Exposure <sup>b</sup> (s)	Airmass <sup>a</sup>	Seeing (arcsec)
2001 07 31	<i>J</i>	52 121.35	30 × 3 × 13	1.25	0.61
2001 07 31	<i>H</i>	52 121.37	15 × 6 × 13	1.22	0.40
2001 07 31	<i>K<sub>s</sub></i>	52 121.40	12 × 6 × 16	1.21	0.39
2001 09 21	<i>J</i>	52 173.22	30 × 3 × 13	1.23	0.49
2001 09 21	<i>J</i>		30 × 3 × 15		0.49
2001 09 21	<i>H</i>	52 173.26	15 × 6 × 13	1.21	0.40
2001 09 21	<i>H</i>		15 × 6 × 14		0.40
2001 11 19	<i>J</i>	52 232.01	30 × 3 × 15	1.40	0.63
2001 11 19	<i>J</i>		30 × 3 × 13		0.63
2001 11 19	<i>H</i>	52 232.05	15 × 6 × 13	1.25	0.48
2001 11 19	<i>H</i>		15 × 6 × 14		0.48
2001 11 20	<i>J</i>	52 233.01	30 × 3 × 15	1.42	0.60
2001 11 20	<i>J</i>		30 × 3 × 13		0.60
2001 11 20	<i>H</i>	52 233.05	15 × 6 × 13	1.26	0.44
2001 11 20	<i>H</i>		15 × 6 × 14		0.44
2001 11 22	<i>J</i>	52 235.01	30 × 3 × 15	1.38	1.00
2001 11 22	<i>J</i>		30 × 3 × 13		1.00
2001 11 22	<i>H</i>	52 235.05	15 × 6 × 13	1.24	0.68
2001 11 22	<i>H</i>		15 × 6 × 14		0.68

<sup>a</sup> Refers to the first exposure.

<sup>b</sup> DIT × NDIT × NEXP.

**Table 5.** Magnitudes of local standards in the near-IR.

Offsets <sup>a</sup>		<i>J</i>	<i>H</i>	<i>K<sub>s</sub></i>
5.34 E	2.23 S	18.10 (0.06)	17.47 (0.03)	17.15 (0.01)
17.04 W	18.25 S	20.23 (0.08)	19.22 (0.06)	18.35 (0.03)
80.87 W	17.36 N	18.45 (0.06)	17.84 (0.02)	17.57 (0.02)
33.98 W	26.71 N	19.87 (0.05)	19.07 (0.04)	18.77 (0.04)
36.80 W	21.81 N	18.30 (0.05)	17.66 (0.03)	17.29 (0.02)
83.25 W	70.93 N	16.08 (0.04)	15.42 (0.01)	15.14 (0.01)
105.06 W	40.36 N	17.54 (0.05)	17.12 (0.02)	17.02 (0.01)
130.73 W	29.53 N	19.03 (0.06)	18.31 (0.03)	18.10 (0.02)
103.50 W	56.17 N	20.37 (0.07)	19.72 (0.07)	19.55 (0.06)
49.27 W	12.32 N	18.29 (0.06)	18.14 (0.03)	17.87 (0.02)
97.35 W	66.92 N	21.13 (0.07)	20.47 (0.07)	20.07 (0.09)
115.60 W	17.95 N	20.94 (0.06)	20.46 (0.07)	20.23 (0.10)
37.25 W	25.82 N	20.37 (0.07)	19.70 (0.05)	19.50 (0.06)
57.13 W	40.81 N	20.01 (0.07)	19.04 (0.04)	18.14 (0.02)

<sup>a</sup> Offsets in arcseconds measured from the supernova.